High Resolution Transmission Electron Microscopic Study of Nanoporous Carbon Consisting of Curved Single Graphitic Sheets

by
L.N. Bourgeois and L.A. Bursill

School of Physics, The University of Melbourne, Parkville VIC 3052 , Australia

ABSTRACT

A high resolution transmission electron microscopic study of a nanoporous carbon rich in curved graphitic monolayers is presented. Observations of very thin regions, including the effect of tilting the specimen with respect to the electron beam, are reported. The initiation of single sheet material on an oriented graphite substrate is also observed.

When combined with image simulations and independent measurements of the density ($1.37 g.cm^{-3}$) and sp^3/sp^2+sp^2 bonding fraction (0.16), these observations suggest that this material is a two phase mixture containing a relatively low density aggregation of essentially capped single shells like squat nanotubes and polyhedra, plus a relatively dense "amorphous" carbon structure which may be described using a random-schwarzite model. Some negatively-curved sheets were also identified in the low density phase.

Finally, some discussion is offered regarding the growth mechanisms responsible for this nanoporous carbon and its relationship with the structures of amorphous carbons across a broad range of densities, porosities and sp^3/sp^2+sp^3 bonding fractions.

§1. INTRODUCTION

The recent synthesis of buckyballs (Kroto *et al.* 1985, Krätschmer *et al.* 1990), carbon nanotubes (Iijima 1991) and similar fullerene-related material such as cones (Iijima 1991) and concentric nested spheres (Ugarte 1992) has stimulated much searching for additional sp^2-carbon structures. In particular, graphitic networks exhibiting negative curvature have been theoretically proposed, such as the tori (Dunlap 1992, Itoh *et al.* 1993) and the low strain schwarzites (Mackay and Terrones 1991, Lenosky *et al.* 1992). Disordered materials associated with fullerenes have also been reported: Ebbesen and Ajayan (1992) noted that glassy-carbon-like materials were synthesized instead of nanotubes when the gas pressure in the deposition chamber was too low; it was also discovered by Tsang *et al.* (1993) that heat treating of the insoluble soot deposited when fabricating buckyballs produced a nanoporous carbon rich in graphitic monolayers. Interestingly, this single-sheet material exhibits striking similarities with the strongly activated anthracite pictured in Millward *et al.* and interpreted as "a series of stacked core-like sheaths" (Millward *et al.* 1978). The pore size of Tsang *et al.*'s carbonaceous material was observed to be of the order of 50 to 150 Å. They suggested that its structure might be related to the random-schwarzite model constructed by Townsend *et al.* (1992), although with lower curvature (Harris *et al.* 1994). Harris *et al.* further pointed out that the nanoporous carbon might be regarded as seeds to multi-layer buckystructures, following its transformation to spherical onions under intense electron irradiation. This suggestion was supported by theoretical calculations on the stability of single and multiple graphitic layers (Bourgeois and Bursill 1996), which predicted that single sheets should have a lower energy than multiple sheets below a size of the order 50 to 500 Å depending on the geometry. The same model also favoured the existence of closed positively curved shells over negatively curved surfaces (Bourgeois and Bursill 1995), when the number of carbon atoms per particle exceeds just a few atoms.

Samples mostly comprised of buckytubes were also found to contain substantial amounts of single graphitic sheets (Bursill and Bourgeois 1995) very similar to the material studied by Tsang *et al.* Other regions were also observed to consist almost entirely of a glassy-carbon-like, multiple-layer compound; but only the monolayer-rich material will be considered in this article; it will be referred to as SSNC or single-sheet nanoporous carbon. The multiple-sheet compound will be the subject of a later publication (Bourgeois and Bursill, *in preparation*). Comparing experimental high resolution images of the bulk of the monolayer porous carbon with image simulations based on the random-schwarzite model of Townsend *et al.* did not preclude the foam-like topology (Bursill and Bourgeois 1995). However, it was clear that the structure of this nanoporous carbon was not determined unambiguously, thus warranting further investigations. Moreover, the presence of these materials in association with buckytubes and buckyparticles, however imperfect they may be, deserved more attention, especially in relation to the nucleation and growth mecha-

nisms responsible for fullerene-related structures. In a parallel study Peng, Fan and Bursill (1996) used parallel electron energy loss spectroscopy (PEELS) to determine the mass density (1.37 g.cm^{-3}) and the sp^3/sp^2+sp^3 bonding fraction (0.16) of this same single-sheet nanoporous specimen.

The purpose of this article is to offer additional information about the structure of the porous carbon using high resolution transmission electron microscopy (HRTEM). In particular, one is interested in determining whether the random-schwarzite model is a reasonable description for this material. The fringe patterns of the images are examined, including the effect of tilting the specimen. HRTEM image simulations performed for a variety of geometries are first presented in order to guide in the interpretation of the fringe contrast and tilting observations. Amorphous carbon was observed as a second component; the structure of this phase is also discussed. In the discussion the HRTEM observations are combined with Peng *et al.*'s measured density and sp^3-bonding character with the aim to clarify the nature of the structures involved.

§2. PROCEDURE

(a) Experimental details

The carbonaceous material which is the subject of this paper was found on the outer ring of a cathode rod kindly supplied by Dr. S. Iijima (NEC Labs., Japan). The cathode was grown using the method of Ebbesen and Ajayan (1992), where a d.c. current is passed between two very pure carbon rod electrodes, resulting in carbon atoms being emitted from the anode onto the cathode. A significant yield of carbon nanotubes and nanoparticles (or bucky-structures) is observed when the deposition vessel is filled with argon or helium at high pressure, of the order of 100-200 Torr (Ebbesen and Ajayan 1992). The samples provided to us were grown in helium atmospheres of 50, 100 and 200 Torr. The deposition performed at 200 Torr gave the best yield in buckytubes and single sheet material.

Only the outer (grey) ring of the cathode contained significant amounts of single sheet material. The middle section (black) was relatively rich in bucky-structures, whereas regions of the cathode close to the core included amorphous material as well as buckytubes.

Small flakes from the desired zone of the sample were crushed in an agate mortar. A clean copper grid was then dipped into the powder, causing tiny specks to stick to the mesh. No solvents were used in the process, a technique which was found to mimimize beam induced artifacts (Bursill *et al.* 1994). The grid was mounted on a tilting stage allowing for -20 to +20° tilts about two orthogonal directions.

HRTEM observations were carried out on a JEOL4000EX instrument operated at 400keV. The point resolution was 1.7 Å with spherical aberration coefficient 0.94mm and optimum defocus of -480 Å. The height of the specimen was constantly adjusted

in order to keep the objective lens current at its optimum value. Care was taken to perform the imaging at optimum defocus; since this is more difficult to realize for single sheets than with multiple-layer structures (Millward 1978), through-focal series of micrographs of a given area were usually taken.

Finally, although beam damage and contamination of the sample appeared quite small, they became evident after a few minutes of beam exposure; this was especially a problem when attempting to obtain tilt series of images for different tilt angles.

(b) Image simulations

Computer-simulated HRTEM images were generated for a variety of graphitic structures for comparison with the experimental images. The objective was to determine image features distinguishing closed surfaces from open ones, and negatively curved sheets from flat and positively curved ones.

The simulations were carried out using an updated version of Melbourne University Multislice (Bursill *et al.* 1990) with parameters adjusted to fit the experimental characteristics of the JEOL 4000EX microscope as stated in section 2(a). Image simulation of finite objects requires them to be placed in unit cells with a certain amount of empty space (typically one quarter of the size of the structure), so that edge effects could be controlled. All the computed images shown below correspond to a defocus value of -500 Å, which is very close to the optimum defocus of our instrument.

§3. RESULTS AND ANALYSIS

(a) Simulated images

The dark lines, seen in the simulations shown in Figs.1-3, correspond to regions of the structures where atoms overlap in projection along the direction of the incident electron beam. Thus "dark loops" can be identified with graphene sheets having a section parallel to the incident electrons. Additional structural information can be inferred from the size and intensity of Fresnel fringes (Millward 1978, Iijima, 1980(b)). These fringes, the result of electrons undergoing Fresnel diffraction at the edges of the specimen, appear as white lines on either side of the black loops. Depending on whether a graphitic layer is flat or curved, and whether it is parallel or lies obliquely with respect to the beam, the white fringes will vary in thickness and intensity. This is illustrated in Figs.1 and 2. Planar sheets will produce symmetrical Fresnel fringes (Fig.1). The main difference between the edge-on case (Fig.1(a)) and the tilted cases (Fig.1(b)-(c)) is the greater contrast in the fringe pattern of the former; this is a consequence of a higher density of atoms in the direction of the beam. In fact, the image contrast rapidly decreases with tilting angle. After a tilting of only 10°, as shown in Fig.1(c), the distinctive black line becomes very faint indeed. As opposed to flat sheets, curved sheets do show a pronounced asymmetry

in their fringe pattern (Fig.2). A positively curved sheet such as a piece of cylinder (Fig.2(a),(b)) or sphere (Fig.2(c)) exhibits a more intense white line on the outer part of the structure, or on the side of the black line corresponding to the larger radius of curvature. The opposite will occur for a piece of negatively curved sheet (Fig.2(d)), i.e. the more intense Fresnel fringe will be on the side of the smaller radius of curvature. A wedge-shaped structure would also produce a fringe contrast similar to a positively curved sheet.

Computed images for the random-schwarzite structure are shown in Fig.3, for two tilting angles of the primitive cell with respect to the electron beam. Further description of these simulations can be found in Bursill and Bourgeois (1995). The curved black lines and their associated Fresnel fringes are characteristic of curved graphitic sections, as discussed above. Note that a difference in tilting angle of only 10° produces noticeable changes. This can be attributed to the rather open nature of R-schwarzite, which is composed of shallow "bowls" rather than almost closed pockets. So tilting the structure by a small amount will change the position of the black fringes representing sections lying more or less parallel to the incident electron beam. This is in contrast with almost closed spheroidal surfaces, for instance, whose simulated images remain almost invariant with tilting.

(b) Experimental HRTEM images

Fig.4 shows an area typical of the single-sheet material. Although most of the porous film displays a complex pattern of overlapping fringe contrast, many well-defined dark loops are visible, especially along the thinnest edges of the specimen. According to the image simulations (Figs.1-3) these loops can be interpreted as curved graphitic sheets having a significant number of atoms (say > 5) overlapping parallel to the incident beam.

In Fig.4 the porous film seems to be terminated by loops only. In some cases a single dark fringe appeared to protrude out of the specimen; however, imaging at a slightly different defocus invariably allowed a "missing" part of the sheet to be found, an example being inset in Fig.4. This suggests that the graphitic sheets are curved and closed, like a sphere (see Fig.2(c)) or a squat tube capped on both ends, rather than just curved and open, like half a cylinder (see Fig.2(b)). Indeed, if the sheets had morphologies similar to the structure shown in Fig.2(b), the resulting HRTEM images would show dangling ends for some orientations of the structure with respect to the beam, assuming of course that the pictured sheets are randomly oriented with respect to the viewing direction.

Some sections of the loops are significantly darker than others, and the adjacent white lines are usually correspondingly brighter (see white arrow in Fig.4). In addition, the white fringe pattern of a loop is often asymmetrical in intensity. In most cases, the brighter fringe lies on the outer side of the loops (see small arrow in Fig.4), which usually corresponds to the side having the larger radius of curvature (see white arrow in Fig.4). The computer-generated images shown in Fig.2 imply

that the imaged structures belong to positively curved surfaces. There are also examples where the more intense fringe is found on the opposite side, i.e. that having the larger curvature; one such case is indicated by a black arrow in Fig.4. These may be identified as negatively curved regions.

Fig.4 shows that the size of the single loops is fairly constant and ranges from approximately 20 to 100 Å, with the most common size $\approx$ 35 Å. A comprehensive study of the size distribution using micrographs from many other regions supported this observation. Overlapping of the structures makes accurate size measurements difficult; however, it was possible to make a simple-minded estimate of the loop size by measuring the apparent width of the protruding objects. Since the aspect ratio of many loops was not one, both characteristic sizes were recorded. The results are shown as a histogram in Fig.5. The majority of characteristic widths is found to range between 25 and 40 Å. The tubular morphology of some loops is also apparent by the small peak at larger sizes, around 80 Å.

Most loops show a distinctly facetted aspect, particularly evident in Fig.4. Furthermore, it should be pointed out that in many instances the junction between two "facets" remains visible, implying that the junction does have a distinct structure, and is not merely a gap.

Many attempts were made to obtain sets of images following a series of tilts about a chosen axis; for example an area similar to Fig.4 was tilted parallel to the edge of the specimen. Fig.6 shows three micrographs taken before tilting (a), after a 10° tilt along the axis indicated by the arrow (b) and after tilting back to the original orientation (c). There are some significant contrast changes from (a) to (c), implying some rearrangement of the graphene sheets during observation; this may be due to some small variation in the diffraction conditions, as it is practically impossible to recover identical orientation and defocus conditions; or to beam heating effects as well as irradiation damage. It also appears that some areas show real changes due to tilting, like the apparent splitting of a dark loop into two dark fringes in (b) (see fat arrow, Fig.6(b)), which then reverts to its original shape in Fig.6(c). Despite this positive result it was concluded that the tilting experiments could not be analysed in detail, due to the difficulty of reliably separating the genuine tilt effects from the beam induced effects. Overall however, very little modification of the image appears to result from tilting, to a 10° angle at least. This can be seen as additional evidence in favour of the loosely-packed aggregate model. In any case this strongly suggests that the layers possess curvatures on the scale of 2-5 nm at least.

The HRTEM simulations for random-schwarzite (Fig.3) clearly show that the fringes are curved on a much smaller scale ($\approx$ 0.3-0.4 nm) than the larger loops of Figs.4,6,7 ($\approx$ 1-2 nm). However, even by scaling up the R-schwarzite structure so that its average radius of curvature is roughly 10-20 Å, its fringe contrast would remain too open compared with the almost closed loops observed experimentally.

Therefore random-schwarzite appears to be a poor representation for the larger sheets.

The existence of an amorphous material (which will be referred to as a-C_*) among the graphitic sheets should be noted. This is evident in all the micrographs, such as the arrowed loops in Fig.4. Some areas of the specimen also showed graphite sheets which appear to be breaking up into very thin layers of amorphous material consisting of highly buckled graphene sheets (Fig.7). Close inspection of Fig.7(a) reveals areas containing both plan and cross-sectional views of graphite, covered with this fine-scale apparently amorphous material just 1-2 nm thick; some details are shown enlarged in Fig.7(b). a-C_* appears to be composed mostly of curved single sheets about 0.5-1nm in size, with radius of curvature on the scale of 0.3-0.5nm. Most of these flakes seem to have dangling edges, distinctly different from the images of larger closed shells. There are also some roughly circular contrasts having diameters of the same order as C_{60}, throughout some of Fig.7. In fact it is interesting to point out that this material is relatively similar to the thin films of amorphous carbon studied by Iijima some fifteen years ago (Iijima 1980(b)); they were interpreted as aggregates of C_{60}-like shells. However, it is our considered judgment that the contrast is modelled very well by R-schwartzite and not by an agglomeration of C_{60} molecules. The simulated images of the random-schwarzite model certainly show good agreement with a-C_*. In particular, the experimental images indicate that the material has a rather open structure, more like R-schwarzite than closed-shell clusters. This does not necessarily imply that the R-schwarzite model should be taken too literally, as will be discussed in the following section. It is also apparent that the density of this "amorphous" material is significantly higher than that of the larger closed shell structures. Careful study of the HRTEM images reveals that most areas, even along the thin edges of the specimen, do contain some "amorphous" phase. Due to the overlap problem for specimens of increasing thickness it is quite impossible to estimate the relative proportions of these two phases. We return to this question in the discussion section below.

Three isolated closed single loops are also visible in Fig.7(a). From the above analysis (and in particular the asymmetrical fringe contrasts), these single loops can be viewed as giant fullerene single shells, in the shape of closed squat nanotubes or polyhedra.

Very few closed loops could be identified unambiguously in Figs.4,6. The thin black arrow in Fig.4 points to a possible complete loop. Much smaller objects, having more or less closed aspect and often attached to larger loops were also sighted. This may be explained by a strong overlap effect. Simple drawings of two superimposed layers of loosely packed circles and ellipses indicate that if their size distribution is relatively large (Fig.8(a)), two objects of very different sizes often overlap in such a way that the smaller loop can be seen in its entirety. But for a narrow size distribution, as seems to be the case of our material, the chance of this happening is very small (Fig.8(b)). This may explain why the overlap is so large even at the

edge of the single-shell aggregate. Fig.8(c) is a sketch of overlapping objects having polyhedral shapes similar to the single loops of Fig.7; comparison with Fig.4 shows that this does give an improved representation of the black fringe distribution in this case. However, the distribution of Fig.8(b) is a better fit for the edge structures of Fig.6.

The presence of some multiple fringe contrasts in the bulk of the specimen should also be noted. The most obvious explanation appears to be that there is a certain percentage of multiple shells in addition to the dominant single-shell objects. An alternative interpretation consists in ascribing double fringes to collapsed shells seen edge-on. The fact that some buckytubes (and presumably any graphitic shell) may fully collapse in order to lower their van der Waals energy has been demonstrated by Chopra *et al.* 1995. The resulting single-sheet object would have one dimension approximately 3.5 Å thick. Seen edge-on, it would result in a two-layer contrast, whereas other viewing directions would show a fatter loop. Hence clusters of these collapsed shells could nicely explain the double-layer fringe patterns; multiple sheets could also arise from the aggregation of two or three collapsed shell sections. Fig.8(d) shows a crude representation for such an aggregate. It is essentially Fig.8(c) with the inclusion of narrow, "dog-bone-like" loops representing collapsed shells seen more or less edge-on. As a result, the overlap effect is more serious than in Fig.8(c). However, no attempt was made in Fig.8 to represent the different contrasts arising from different thicknesses along the electron beam direction. Fig.8(a) and Fig.8(d) depicting objects of widely varying sizes, they are not expected to be realistic representations of HRTEM images. Specifically to Fig.8(d), the contrast of the wider loops, arising from the narrow sides of the shells (about the size of C_{60}) should be quite low. This is not consistent with the relatively strong contrast observed in the experimental images. Furthermore, no "dog-bone-like" loops were seen to protrude out of the edge of the specimen. Nevertheless, one cannot discount the possibility that the small amount of double fringes present in the monolayer material may be caused by partially or fully collapsed shells seen edge-on; the collapsed sections of such structures viewed from other directions should be expected to be virtually invisible.

In conclusion, we suggest that the larger loops represent closed single shells, the majority of them being inflated polyhedral or spheroidal objects; a relatively small proportion of shells in various stage of collapse due to the van der Waals forces between opposite walls may also be present. This interpretation is at odds with previous suggestions of multiply-connected random surface. An amorphous phase whose HRTEM images could be accounted for by a random-schwarzite-like structure was found interspersed in the closed shell aggregates.

§4. DISCUSSION

(a) Density considerations

The density of several models of aggregated spherical carbon shells was estimated. The shells were assumed to have the same size and to exhibit dense random packing with an inter-shell separation of 3.2 Å, as in solid C_{60}. Using a dense random packing efficiency equal to 0.8 times that of face-centered cubic packing (Elliott 1983) we obtained densities of 0.7 and 0.5 g.cm^{-3} for single shells respectively 30 and 50 Å in diameter. Double shells were calculated to result in densities of 1.4 and 1.0 g.cm^{-3} for the above sizes. Clusters of collapsed, "pancake-shaped" single shells were also modelled, and the density estimated. Due to their flattened aspect, the objects may pile up in a fairly orderly fashion with their broad dimension aligned in the same direction; this semi-ordered arrangement will be referred to as the "pile" structure . A maximum density of 1.3 g.cm^{-3} is then deduced for a shell radius of 30 Å. If on the other hand the shells are randomly oriented in all three directions, the resulting aggregate will exhibit a low density of 0.24 g.cm^{-3} for the same shell radius. These densities are tabulated in Table 1 together with those for random-schwarzite and Beeman *et al.*'s C340 model for amorphous sp^2 carbon. This is to be compared with the value of 1.37 g.cm^{-3} deduced from PEELS (Parallel Electron Energy Loss Spectroscopy) analysis of the porous material (Peng *et al.* 1996) — see Table 2. Only the "pile" model for collapsed single shells and a cluster containing 100 % of double shells yield values in good agreement with the experimental result. These two aggregates appear unlikely to account for the entire material observed. Although a small percentage of multiple-layer structures (inflated or collapsed) is certainly present in the monolayer material, this alone is unlikely to increase the density to the experimental value of 1.4 g.cm^{-3}. But the presence of a-C_* has not yet been taken into account. By describing amorphous carbon as a random packing of C_{60} particles, it is found to have a density of 1.35 g.cm^{-3}. Incidently, this value is not very different from that of random-schwarzite, 1.26 g.cm^{-3} (Townsend *et al.* 1992). However, this is still slightly lower than the measured density for the two combined phases. This strongly suggests that a-C_* is much denser than either an aggregate of C_{60}, or R-schwarzite. The a-C_* phase may also be compared with other types of amorphous carbon. For example, evaporated amorphous carbon (E.a-C) appears very similar to a-C_* under HRTEM (Peng *et al.* 1996); it is dominated by sp^2-type bonds and has a density of 2 g.cm^{-3}. Assuming that a-C_* has a density close to 2 g.cm^{-3}, a volume fraction of less than 30% (associated with 70% of 40 Å-wide inflated single shells) would suffice to reproduce the measured density value.

From these considerations it is confirmed that SSNC is made of two phases, a relatively low density one comprised predominantly of inflated single shells, with a small percentage of multiple-layer structures and collapsed objects, and a higher density phase similar to evaporated amorphous carbon. Experimental data on the $sp^3/(sp^2+sp^3)$ bonding fraction is presented in the following section in order to further this interpretation.

(b) sp^3/sp^2+sp^3 ratio

A graphitic surface only contains three-fold coordinated atoms normally and hence would appear to be purely sp^2-bonded. However, it was shown by Haddon (1993) that curvature of the graphitic network will introduce some degree of sp^3-bonding. In solid C_{60} (C_{60} being the smallest curved surface to be stable) the sp^3/sp^2+sp^3 ratio was measured to be only a few percents (Hawkins *et al.* 1991, Peng *et al.* 1996). This places a higher limit on the amount of sp^3-bonding resulting purely from curvature. Pure sp^3-bonds may also be present in a predominantly sp^2-bonded structure; high-curvature junctions would seem an ideal location for tetrahedral bonds because of the large strain. The junction structure of the closed shell aggregate is now discussed.

Most loops in the single-shell phase were found to be polygons, with the sharp junctions clearly imaged. These junctions can either correspond to a twin-like connection (i.e. a wedge) or to a cone-like structure seen on its side. The second case can be interpreted in terms of non six-rings (Iijima 1991). Finding a reasonable junction structure for the twin-like case appears difficult since the observed angles are small; the angle between graphite twin planes is usually no larger than about 20 degrees, equivalent to a wedge angle of 160° (Kelly 1981). Tetrahedral bonding was suggested as a possible way of obtaining twin angles of the order of 60 to 80° (corresponding to wedge angles of 120 to 140°) (Iijima 1980(a), Hiura *et al.* 1994). But such links would leave out some bonds; it seems unlikely that so many dangling bonds would have been created in the inert environment in which our material was formed. Hence the favoured model regarding the structure of the single shells appears to be a graphitic lattice curved into a close surface through the introduction of non six-rings. If on the one hand these non six-rings are few and isolated, they will result in a polyhedron. For instance the ground state structure of fullerenes contains twelve isolated pentagons; it is clearly polyhedral for the larger shells (C_{540}, C_{960} ...etc). Structures of this type, but probably not as symmetrical, are good candidates for most of our observed polyhedral objects (see the single shells in Fig.7 in particular). On the other hand, inclusion of many non six-rings such as pentagons and heptagons into the graphitic network will produce smoothly curved shells, resembling the spheroids described as the high temperature equilibrium structures of fullerenes (Maiti *et al.* 1993) — see Fig.6.

These observations have important implications regarding the degree of sp^3-hybridisation of the compound. The single-shell phase having a much lower curvature than C_{60}, it is expected to show a much smaller sp^3-to-sp^2 fraction, less than one percent. However Peng *et al.* found an $sp^3/sp^2+ sp^3$ ratio of 16 % (see Table 2). This suggests that most of the sp^3 character of the material originates from the amorphous phase. Evaporated amorphous carbon having been measured to contain 14 % of sp^3-type bonding (Peng *et al.* 1996) — see Table 2, a close structural similarity between a-C_* and E.a-C seems quite plausible. This point will now be addressed.

(c) A model for a-C$_*$

The texture of a-C$_*$ observed by HRTEM was found to be modelled quite satisfactorily by R-schwarzite. But arguments presented above imply that the density and the sp^3-to-sp^2 ratio of a-C$_*$ must be significantly higher than that the pure sp^2 random surface models. In order to account for these characteristics of a-C$_*$, the following model is proposed: a foam-like topology, comprised of positively and negatively curved regions, and with sp^3-bonds where curvature is too high for the trigonal environment to be retained. This would result in a continuous network with a predominantly two-dimensional aspect and some bifurcations of the surface caused by sp^3-bonds. Beeman *et al.* constructed several models for amorphous carbons having different sp^3-to-sp^2 ratios (Beeman *et al.* 1984). The model having the closest percentage of four-fold coordinated atoms with respect to a-C$_*$, referred to as C340 by Beeman *et al.*, contained small, curved graphitic sheets interconnected via sp^3 bonds. It was found to have a density of 2.69 g.cm^{-3}. This is significantly higher than that of E.a-C. However, the curvature of the sp^2-bonded regions could easily be decreased (by changing the number and types of non six-rings) in order to increase the porosity of the structure, thus decreasing the density.

An energetics study of curved graphitic surfaces in an environment of high dangling bond energy (Bourgeois and Bursill 1995) showed that for very small sheets, i.e. having less than about 35 atoms, positive and negative curvature result in little difference in energy. In the light of these results, a random-surface model, necessarily composed of many negatively curved regions, appears to be a good description for a material curved on the scale of 0.3-0.4nm. Another prediction of the theoretical analysis by Bourgeois and Bursill was the increasing stability of positively curved surfaces with respect to their negatively curved counterparts as size increases. This is consistent with the closed shell geometry observed for the larger objects described in this article.

It is still unclear what the parameters controlling the porosity/density are. Some suggestions will nevertheless be made in the following section.

(d) Nucleation of single-shell material

The intimate connection between the closed shell aggregates and the a-C$_*$ phase suggests that the latter may serve as nuclei for the larger objects. A similar idea was put forward by Iijima *et al.* (1991) regarding the role of amorphous carbon commonly found on buckytubes. The following mechanism for the formation of the amorphous phase may be proposed: provided the nucleation rate is much faster than the growth rate, many very small sheets may form on the surface of the cathode, with comparable amounts of positive, negative and zero curvature (in agreement with our energetics model). Eventually they will overlap; bridging of the "islands" in order to eliminate dangling bonds may then be accomplished via additional bits of curved surfaces and sp^3 bonds. The resulting structure would be C340-like (or R-schwarzite-like with sp^3 bonds). The abundance of non six-rings in this material

makes it ideal for the nucleation of larger, curved graphitic sheets. However, the development into closed shells should be expected to follow from a slowing down of the kinetics. In this picture, a-C_* is then the material leftover in the growth of the larger shells.

§5 CONCLUSION

The detailed structure of a nanoporous carbon film found in association with fullerene-related material was studied by HRTEM. Strong evidence was presented showing that this film consisted of closed single shells some 30 to 100 Å in size, rather than a multiply-connected random surface. The dominant morphology of the single sheets was found to be polyhedral, similar to the ground state structure of giant fullerenes; the possibility that some of the shells have partially or fully collapsed was proposed. A significant amount of amorphous carbon was also observed on top or inside the shells, and on the surface of thin graphite planes. HRTEM images showed it to consist of curved graphitic flakes as small as a few angstroms. Combined with considerations about the density and degree of sp^3 character, these observations appeared to favour a negatively curved random-schwarzite model for the amorphous carbon phase.

ACKNOWLEDGEMENTS

This work was supported financially by the Australian Research Council. We wish to acknowledge the use of the HRTEM facility at the University of Melbourne, part of the National Advanced Materials Analytical Centre (NAMAC). We are also grateful for the cooperation of Dr. S. Townsend, who provided the atomic co-ordinates for R-schwarzite. L.N.B. acknowledges the support of an ARC funded Australian Post-Graduate Research Award.

REFERENCES

BEEMAN, D., SILVERMAN, R., LYNDS, R. and ANDERSON, M.R., 1984, *Phys. Rev.* B, **30**, 870.

BOURGEOIS, L.N. and BURSILL, L.A., 1995, *Int. J. Mod. Phys.* B **9**, 3319.

BOURGEOIS, L.N. and BURSILL, L.A., 1996, *Int. J. Mod. Phys.* B **10**, 563.

BURSILL, L.A. and BOURGEOIS, L.N., 1995, *Mod. Phys. Lett.* B **22**, 1461.

BURSILL, L.A., PENG, J.L. and FAN, X.D., 1990, *Int. J. Mod. Phys.* B **4**, 273.

BURSILL, L.A., STADELMANN, P.A., PENG, J.L. and PRAWER, S., 1994, *Phys. Rev.* B **49**, 2882.

CHOPRA, N.G., BENEDICT, L.X., CRESPI, V.H., COHEN, M. L., LOUIE, S.G. and ZETTI, A., 1995, *Nature*, **377**, 135.

DUNLAP, B.I., 1992, *Phys. Rev.* B **46**, 1933.

EBBESEN, T.W. and AJAYAN, P.M., 1992, *Nature*, **358**, 220.

ELLIOTT, S.R., 1983, *Physics of amorphous materials* (Longman), p324.

HADDON, R.C., 1986, *J. Am. Chem. Soc*, **108**, 2837.

HARRIS, P.J.F., TSANG, S.C., CLARIDGE, J.B. and GREEN, M.L.H., 1994, *J. Chem. Soc., Faraday Trans.*, **90**(18), 2799.

HAWKINS, J.M., LOREN, S., MEYER, A. and NUNLIST, R., 1991, *J. Am. Chem. Soc.*, **113**, 7770.

HIURA, H., EBBESEN, T.W., FUJITA, J., TANIGAKI, K. and TAKADA, T., 1994, *Nature*, **367**, 148.

IIJIMA, S., 1980(a), *J. Cryst. Growth*, **50**, 675.

IIJIMA, S., 1980(b), *J. Microsc.*, **119**, 99.

IIJIMA, S., 1991, *Nature*, **354**, 56.

ITOH, S. and IHARA, S., 1993, *Phys. Rev.* B **48**, 8323.

KELLY, B.T., 1981, *Physics of graphite* (Applied Science Publishers).

KRÄTSCHMER, W., LAMB, L.D., FOSTIROPOULOS, K. and HUFFMAN, D.R., 1990, *Nature*, **347**, 354.

KROTO, H.W., HEATH, J.R., O'BRIEN, S.C., CURL, R.F. and SMALLEY, R.E., 1985, *Nature*, **318**, 162.

LENOSKY, T., GONZE, X., TETER, M. and ELSER, V., 1992, *Nature*, **355**, 333.

MACKAY, A.L. and TERRONES, H., 1991, *Nature*, **352**, 762.

MAITI, A., BRABEC, J. and BERNHOLC, J., 1993, *Mod. Phys. Lett.* B **7**, 1883.

MILLWARD, G.R., JEFFERSON, D.A. and THOMAS, J.M., 1978, *J. Microsc.*, **113**, 1.

PENG, J.L., BURSILL, L.A. and FAN, X.D., 1996, *Int. J. Mod. Phys.* B **10**, 3875.

TOWNSEND, S.J., LENOSKY, T.J., MULLER, D.A., NICHOLS, C.S. and ELSER, V., 1992, *Phys. Rev. Lett.*, **69**, 921.

TSANG, S.C., HARRIS, P.J.F., CLARIDGE, J.B. and GREEN, M.L.H., 1993, *J.Chem. Soc., Chem. Commun.*, 1519.

UGARTE, D., 1992, *Nature*, **359**, 707.

FIGURE CAPTIONS

Figure 1:
Computer image simulation for a 30 Å square flat graphite sheet (a) viewed edge on, (b) viewed 5 degrees from edge on, and (c) viewed 10 degrees from edge on.

Figure 2:
Image simulations of (a) a 21 Å wide carbon tube capped at one end by half a C_{540} shell. The long axis of the tube is perpendicular to the electron beam, i.e. it lies in the viewing plane; (b) half the structure of (a), cut longitudinally; (c) a C_{540} shell seen near its five-fold axis; (d) a piece of negatively curved graphitic sheet.

Figure 3:
Simulated images of one primitive cell of the random-schwarzite model for two different orientations with respect to the incident electrons. The difference in tilt angle between (a) and (b) is 10°.

Figure 4:
HRTEM micrograph showing a region typical of the porous sp^2-carbon found in conjunction with buckytubes and polyhedral particles. The small arrow shows an example of asymmetrical fringe pattern; the large black arrow points to a possible negatively curved region; the white arrow indicates a high contrast loop.

Figure 5:
Histogram showing the size distribution of the loops visible on the edge of the specimen.

Figure 6:
Micrographs showing (a) a single-sheet region before tilting, (b) after a 10° tilt as indicated by the arrow (the tilt axis is perpendicular to that arrow), (c) and after tilting back to the original orientation. The fat arrow in each picture points to the same loop, splitting in two in (b).

Figure 7:
(a) Isolated single loops among thin graphite ribbons. (b) Enlargement of (a) showing greater detail of the amorphous material.

Figure 8:
Schematic diagram showing two overlapping layers of (a) ellipses of variable size and aspect ratio, (b) ellipses of almost constant size and aspect ratio, (c) polygons of similar size and aspect ratio, (d) polygons of similar size but different aspect ratio.

model	density ($g.cm^{-3}$)	$sp^3/(sp^2 + sp^3)$ bonding fraction
ISSA	0.5-0.7	0
IDSA	1.0-1.4	0
CSSA	0.24-1.3	0
C340	2.69	0.09
R-schwarzite	1.26	0

Table 1: Mass density and $sp^3/sp^2 + sp^3$ bonding fraction of several models for amorphous carbon. C340 is due to Beeman *et al.* 1984 and R-schwarzite to Townsend *et al.* 1992. ISSA is the inflated single-shell aggregate model, and IDDA the double-shell equivalent. CSSA corresponds to the collapsed single-shell aggregate model.

material	density ($g.cm^{-3}$)	$sp^3/(sp^2 + sp^3)$ bonding fraction
SSNC	1.37	0.16
Evaporated a-C	2.07	0.14
CVD a-C	3.51	1
solid C_{60}	1.71	0.08
graphite	2.28	0
diamond	3.52	1

Table 2: Measured mass density and $sp^3/sp^2 + sp^3$ bonding fraction for several carbon materials (Peng *et al.* 1996); CVD a-C stands for chemical vapour deposited amorphous carbon and SSNC for single-sheet nanoporous carbon. Solid C_{60}, graphite and diamond are also included for comparison.

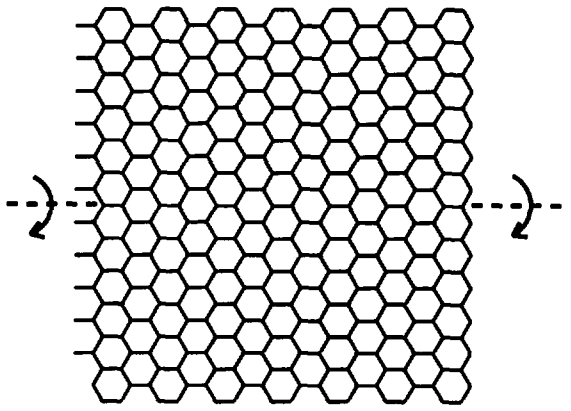

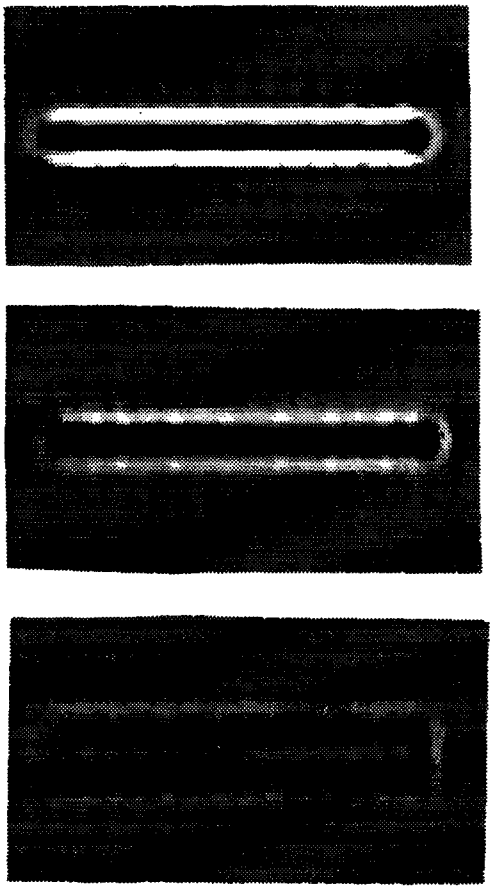

(a)

(b)

(c)

1nm

FIG. 1

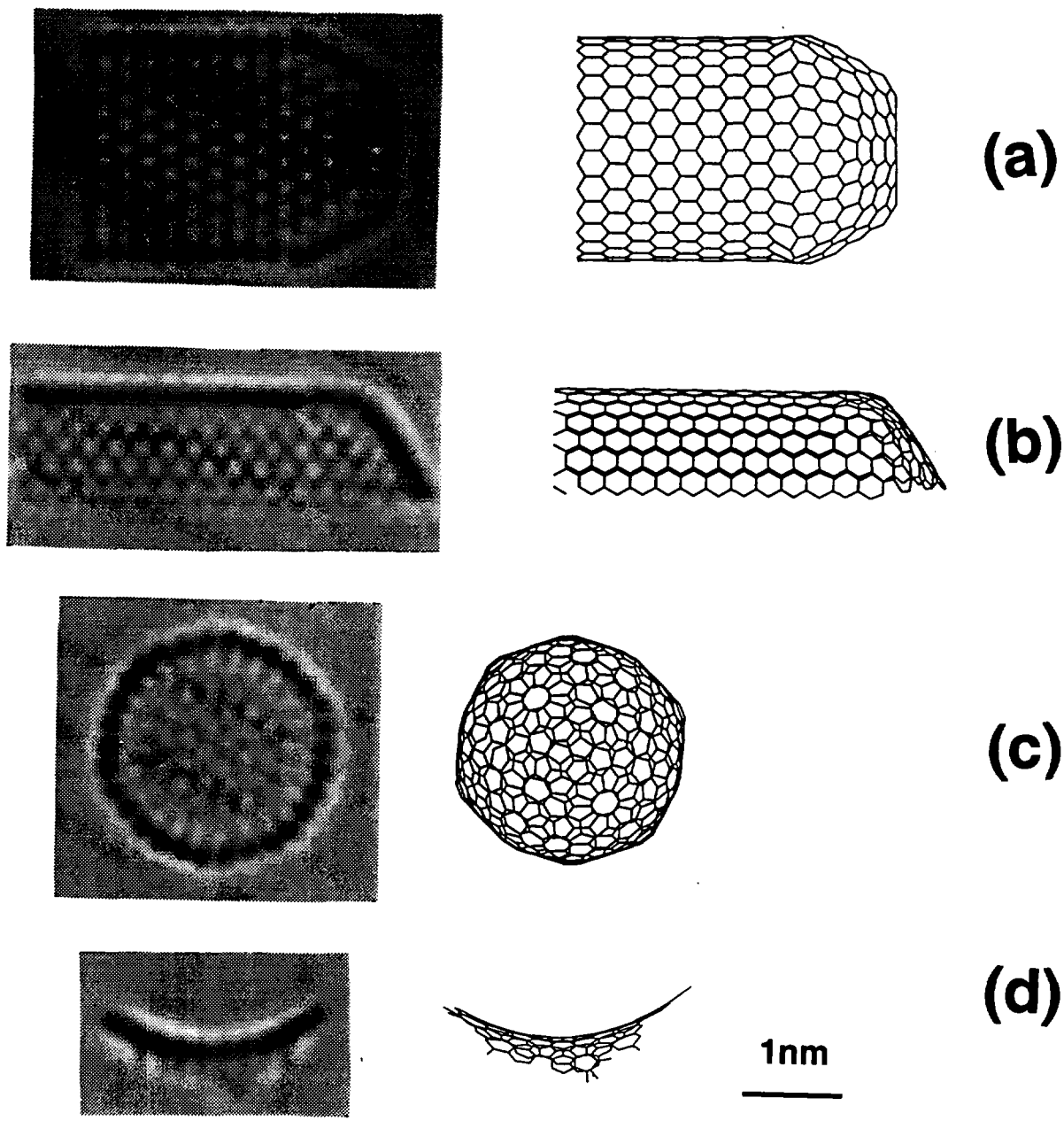

FIG. 2

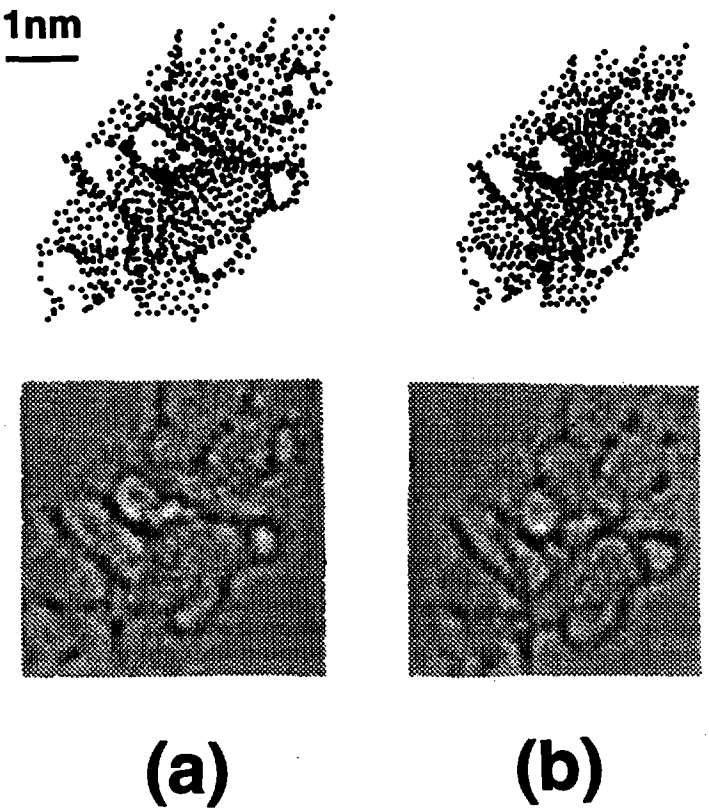

FIG. 3

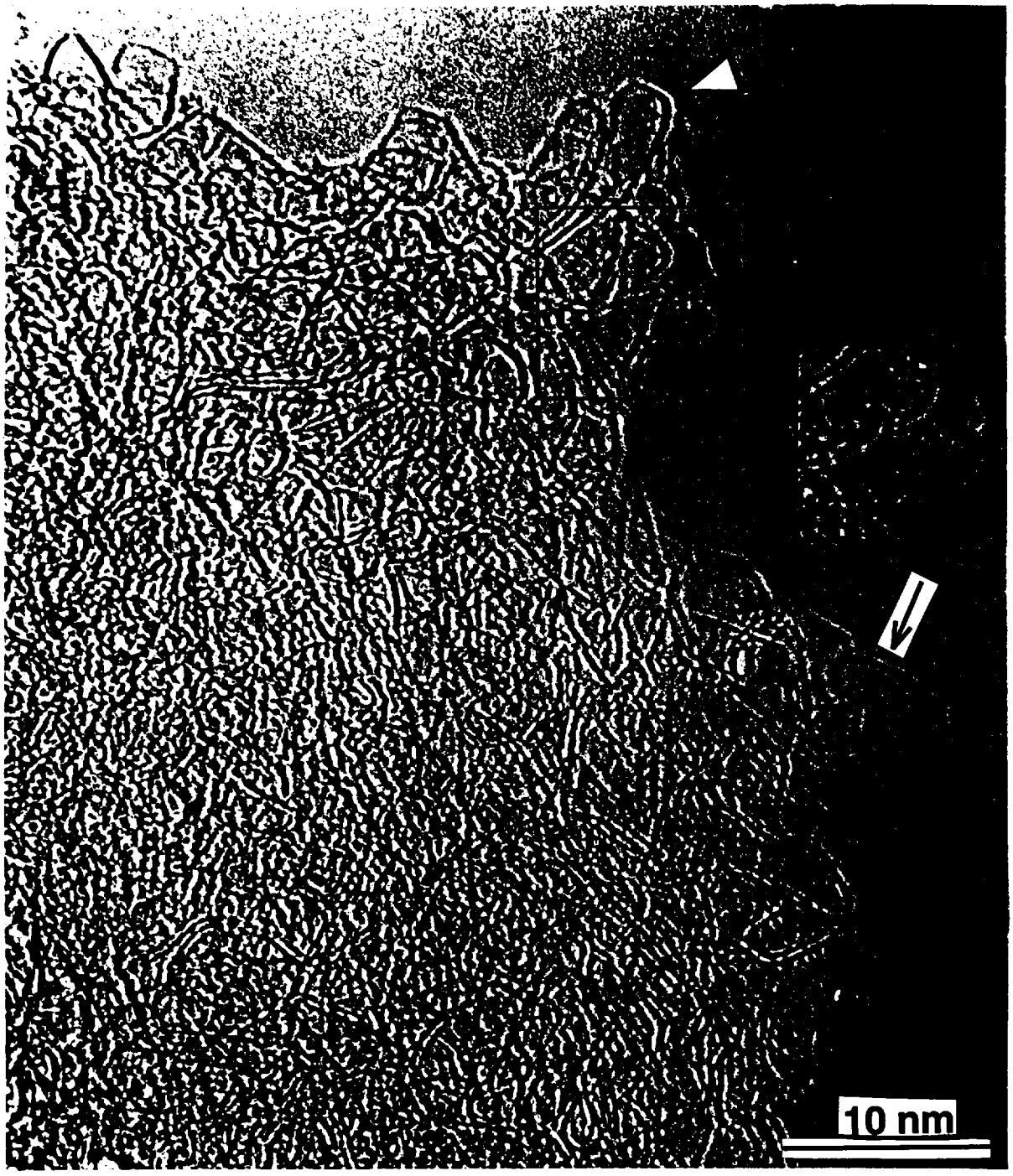

FIG. 4.

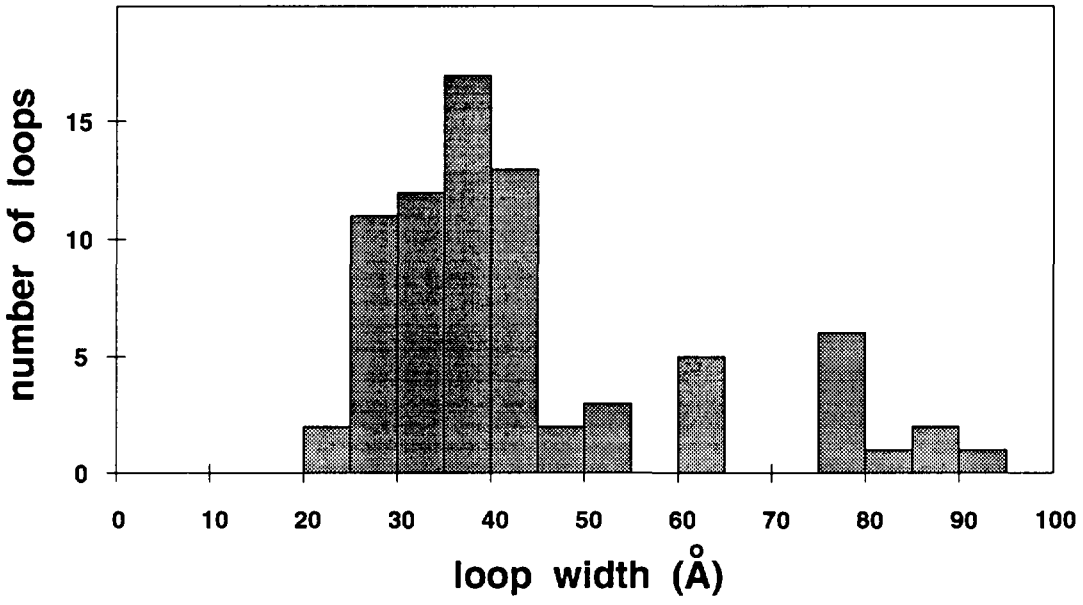

Figure 5: Histogram showing the size distribution of single loops visible on the edge of the specimen.

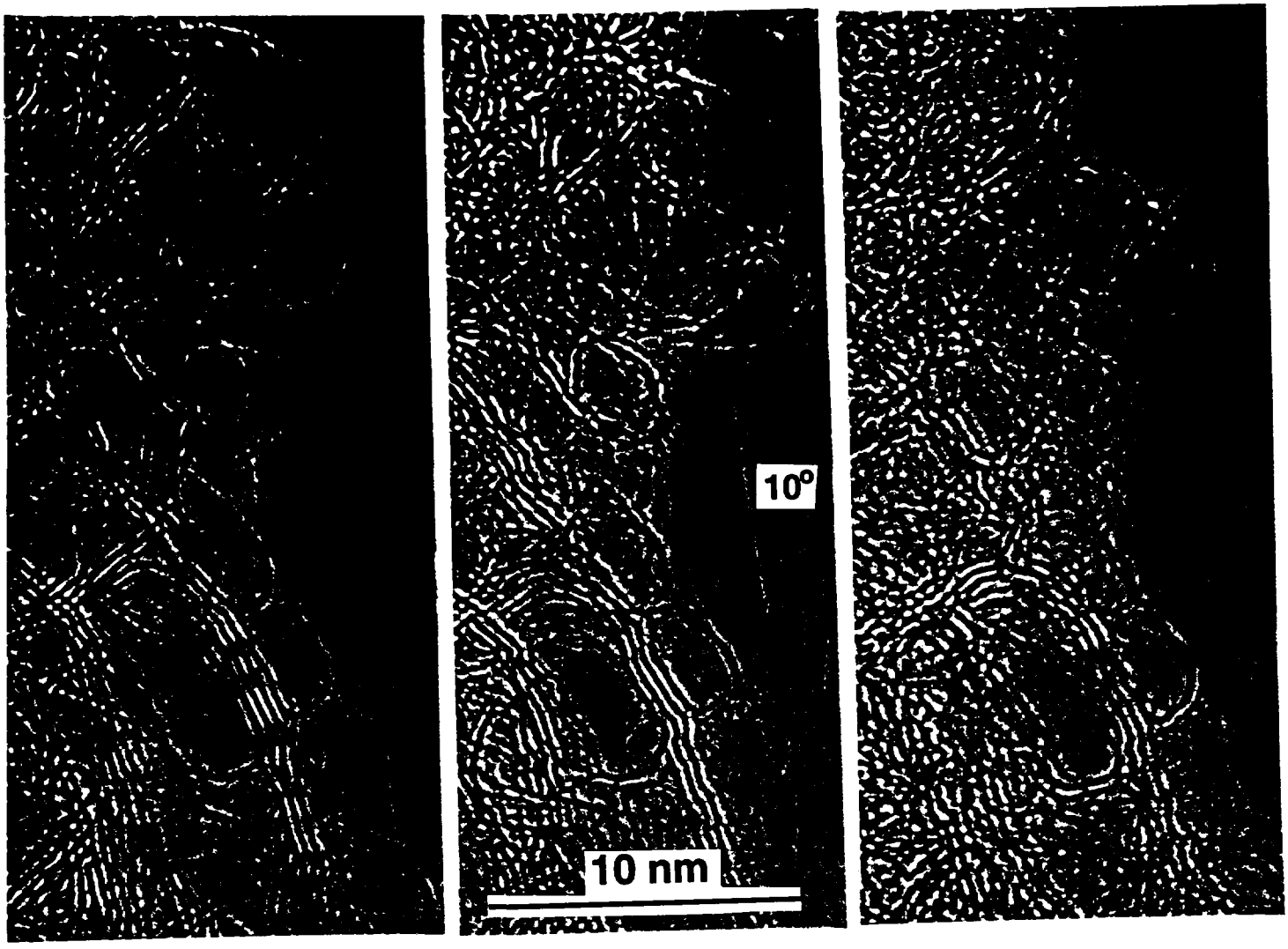

FIG. 6

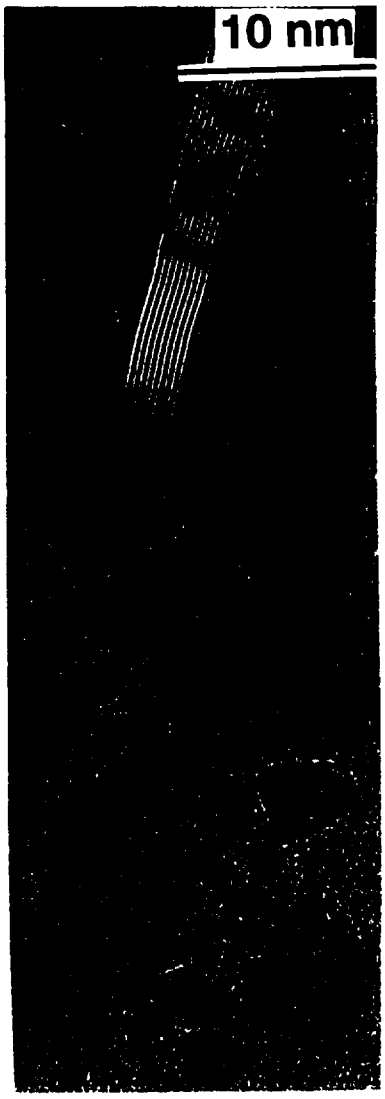

(a)

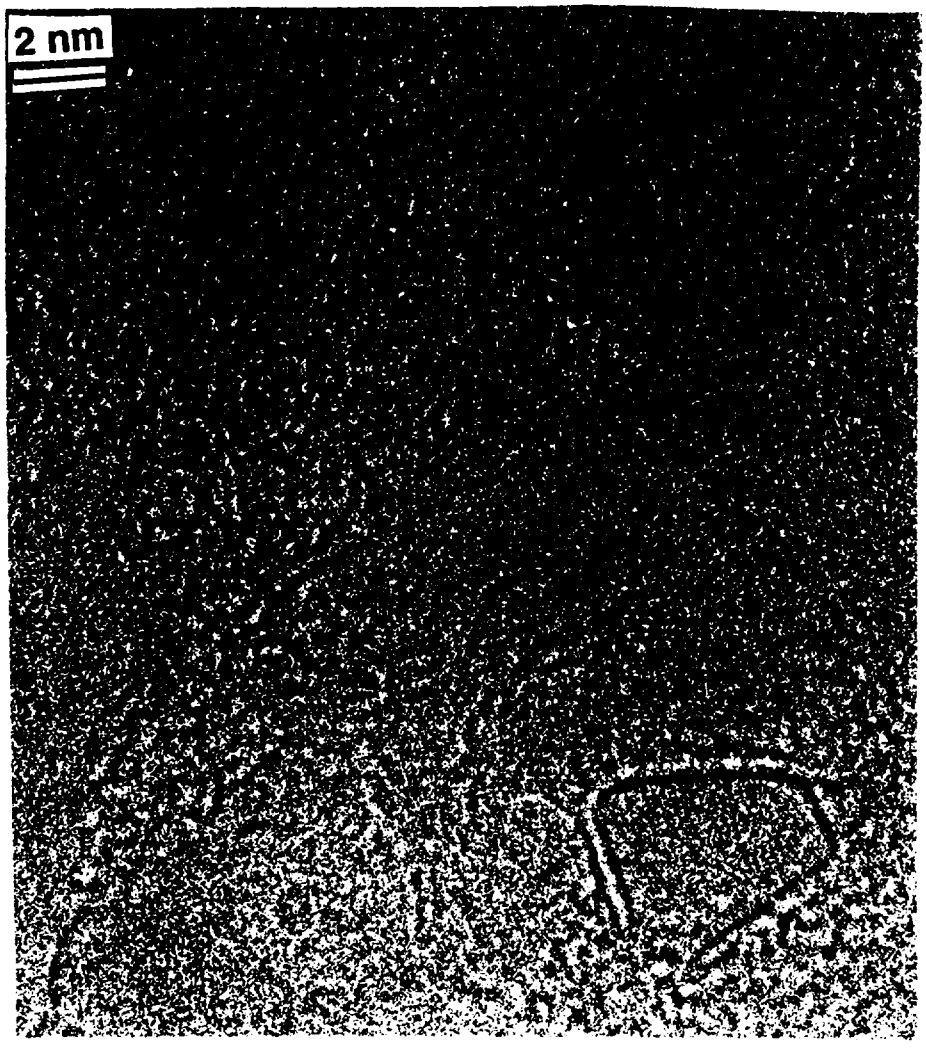

(b)

FIG. 7

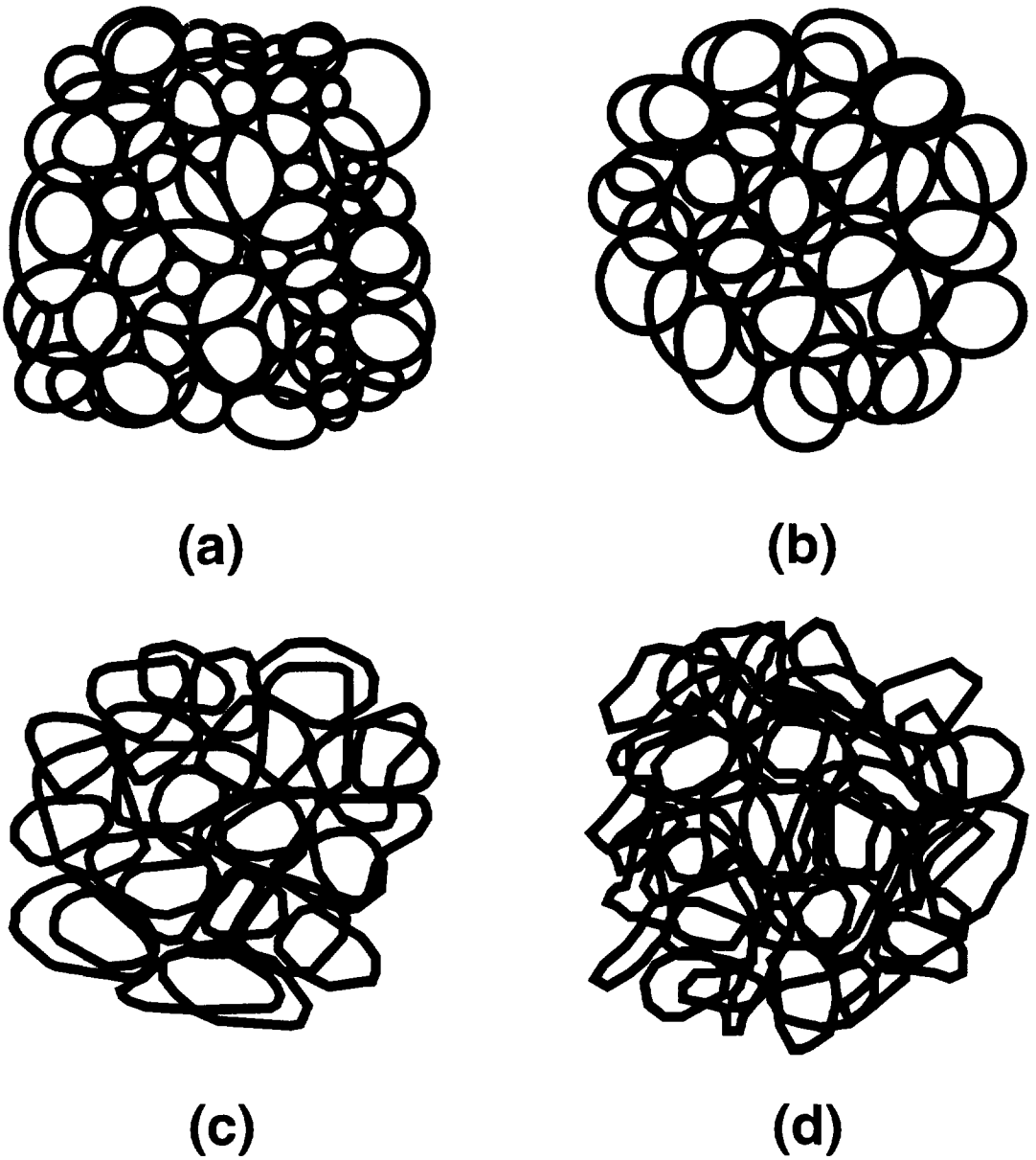

Figure 8: Schematic diagram showing two overlapping layers of loosely packed (a) ellipses of variable size and aspect ratio, (b) ellipses of similar size and aspect ratio, (c) polygons of similar size and aspect ratio, (d) polygons of similar size but different aspect ratio.